Scientia Iranica B (2014) 21(5), 1635–1642

Sharif University of Technology
Scientia Iranica
Transactions B: Mechanical Engineering
www.scientiairanica.com

Performance of piezoelectrically actuated micropump with different driving voltage shapes and frequencies

E.M. Kolahdouz[a], K. Mohammadzadeh[b], E. Shirani[b,*] and S. Ziaei-Rad[c]

a. *University at Buffalo, Department of Mechanical Engineering, Buffalo, NY, 14260.*
b. *Foolad Institute of Technology, Fooladshahr, Isfahan, P.O. Box 84916-63763, Iran.*
c. *Department of Mechanical Engineering, Isfahan University of Technology, Isfahan, P.O. Box 84156-83111, Iran.*

Received 20 June 2012; accepted 26 February 2014

KEYWORDS
Micropump;
Nozzle-diffuser;
Waveform;
Vorticity;
Frequency.

Abstract. The effects of driving voltage waveform and frequencies on the performance of a piezoelectrically actuated micropump are investigated in detail. A full three-dimensional piezoelectric micropump was modeled numerically and tri electro-mechanical-fluidic coupling effects have been taken into account on its interface boundaries. Standard excitation waveforms including sinusoidal, triangle, sawtooth and square shapes were implemented and the results were compared with each other. The real time pump flow behavior was studied in each case for different membrane positions. The analysis predicts that the more sharp jump in the wave form, the more pump flow can be attained at the outlet. Square shape excitation with the sharpest instantaneous slope has the most notable overall flow rate compared to the other types in the examined range of frequencies. The behavior can be explained by considering the generated vortices in the flow. Due to a sudden jump in membrane position, the flow forms strong vortices, which magnify the diodicty of the valves.

1. Introduction

Microelectro mechanical systems (MEMS) have been one of the most favorite research topics over the last two decades. It is possible to fabricate compact and high performance systems for delivering, manipulating, analyzing or processing small amounts of liquid flow in chemical and biological applications. Micropump devices, especially, play a very important role in every microfluidic network system. Among various types of micropump, the valve-less type is more attractive to scientists, due to its scalability, durability, and simplicity of fabrication.

*. *Corresponding author.*
E-mail addresses: mkolahdo@buffalo.edu (E.M. Kolahdouz); kazem.mohamadzadeh@gmail.com (K. Mohammadzadeh); eshirani@ictp.it (E. Shirani); szrad@cc.iut.ac.ir (S. Ziaei-Rad)

Furthermore, a robust way to handle particle-laden flows is to use No-Moving-Parts (NMP) valves that allow the free passage of particles and rely on fluidic instead of mechanical parts to inhibit reverse flow. The possibility of working under high frequency conditions is another advantage of using NMP valves. In summary, the valve-less micropump helps designers to test the pump condition under a wide range of frequency domain. It is also possible to choose different wave shape forms for periodic excitation. In this study, the main aim is to analyze micropump performance under different conditions of driving voltage waveforms and frequencies.

Incorporating nozzle-diffuser microvalves was first realized by Stemme and Stemme in 1993 [1]. Forster et al. [2], in 1995, used valvular conducts as check valves in the piezoelectric micropump. They also experimentally tested their micropump under harmonic and square wave excitation applied to the driver amplifier, and the importance of the waveform shape was indicated. It was proven that even the peak excitation voltage was the same for harmonic and square wave excitations; the pump output being significantly larger for the latter. Olsson et al. [3], in 1998, used square wave excitation voltage; the resulting diaphragm motion was measured using a fiber-optical detection system. Since the pump worked close to resonance frequency, the diaphragm vibration was sinusoidal in time, rather than a square wave.

Studies conducted by other researchers [4,5], in 2000 and 2001, analyzed the valveless piezoleectric micropump. They calculated the natural frequency and showed that there is a linear relation between the flow rate and head pressure at a constant driving voltage. As micropump design and analysis is a complicated multidisciplinary problem with various field couplings, many research studies have been conducted to optimize the piezoelectrically actuated valveless micropump design [6,7,8]. Most of this research, however, underestimated the interaction effects of diaphragm vibration and fluid flow. Yang et al. [9], in 2008, used the commercial software, ACE, and investigated the influence of frequency, opening angle, geometric dimension and membrane amplitude on the performance of a square chamber micropump. However the effects of the structural part, including piezoelectric influence, were not directly simulated, and mesh displacement of the chamber was modeled using the multiplication of three harmonic functions of x, y and t. Hou et al. [10], in 2008, analyzed the mechanical properties of a diaphragm involved in the piezoelectric micropump. The displacement of the membrane center was reported under different driving voltage and PZT thickness. Nevertheless, a two-way interaction between the fluid and solid parts was not studied. Cui et al. [11], in 2008, studied the whole micropump using ANSYS software. The completed coupled-field simulation was studied for the valveless micropump using a finite element model. In their work, the effects of geometry on micropump characteristics were analyzed, even though the frequency was constant and far from the first natural frequency of the system. Yanfang et al. [12], in 2009, introduced a piezoelectric micropump with a saw-teeth microchannel. They fabricated and tested this micropump against the traditional diffuser and showed that their saw-teeth micropomp produces higher maximum flow rate. They also tested the pump with different driving voltages and frequencies under the sine, square and ramp signal. They were only able to show the maximum flow rate and maximum pressure head of the pump.

The pump's performance obviously depends on the shape of the waveform. As far as the authors of this work are concerned, there have been no numerical studies of the waveform effect on flow behavior in a micropump. The experimental work, some of which are mentioned above, can only produce some global results, such as maximum flow rate or head, with some degree of accuracy. This is mainly due to limitations on the measurement devices and experiments. Thus, the details of the flow, such as instantaneous velocity and flow rate, and flow structure inside the micropump, cannot be obtained by experiments accurately and, thus, are not presented. The aim of this work is to simulate 3-D flow inside micropumps and study the flow structures to understand and obtain further insight regarding micropump performance when the driving voltage waveform and frequencies are changed. In this paper, the effects of driving voltage waveform on the performance of a piezoelectrically actuated micropump are investigated using a three-dimensional model, considering a tri electro-mechanical-fluidic coupling. Details of the flow inside the micropump are presented and discussed.

2. Governing equations and numerical method

2.1. Fluid flow

The flow was assumed to be laminar, incompressible and Newtonian. Conservation equations for mass and momentum in the Cartesian coordinate can be expressed as unsteady three-dimensional Navier-Stokes equations:

$$\rho_f \frac{\partial U_i}{\partial t} + \rho_f \frac{\partial}{\partial x_j}(U_j U_i) = -\frac{\partial P}{\partial x_i} + \frac{\partial}{\partial x_j}\left(\mu_f \left(\frac{\partial U_i}{\partial x_j} + \frac{\partial U_j}{\partial x_i}\right)\right), \tag{1}$$

and equation of continuity:

$$\frac{\partial U_j}{\partial x_j} = 0, \tag{2}$$

where U is the velocity vector, x demands for direction, ρ_f is the density of fluid, μ_f is the fluid viscosity, P is the pressure, and indexes, i and j, indicate the 3-D coordinate directions. These equations are integrated over a control volume and discredited with the finite volume based technique to be used in the numerical solution process. Second Order Backward Euler is used for discretization of transient terms. Advection terms are discretized using a high resolution scheme, which is a bounded second-order upwind biased discretization. A co-located grid layout was used. However, various terms in the equations require solutions or solution gradients to be approximated at integration points. Finite element shape functions are, consequently, used to evaluate the solution and its variations within mesh elements.

2.2. Structural part

Considering transient dynamic analysis for the structural part, the basic equation of motion can be expressed according to Newton's second law:

$$\boldsymbol{\sigma}_{ij,j} + \mathbf{f}_i = \rho_s \ddot{\mathbf{u}}_i, \tag{3}$$

where $\boldsymbol{\sigma}$ is the stress tensor, $\mathbf{f}$ is the body force, ρ_s is the density and $\mathbf{u}$ is the displacement vector. The relationship between the strains and the displacements and charge equation of electrostatics, are:

$$\varepsilon_{ij} = (u_{i,j} + u_{j,i})/2, \tag{4}$$

$$D_{i,i} = 0, \tag{5}$$

$$E_i = -\phi_{,i}. \tag{6}$$

Here, $\boldsymbol{\varepsilon}$ is the strain tensor, D is the electric displacement vector, $\mathbf{E}$ is the electric field and Φ is the electrical potential.

In linear piezoelectricity, the equations of elasticity are coupled to the charge equation of electrostatics by means of piezoelectric constants. Therefore, piezoelectric constitutive equations can be expressed in strain-charge form as:

$$\boldsymbol{\sigma}_{i,j} = C^{\mathbf{E}}_{ijkl}\varepsilon_{kl} - e_{kij}\mathbf{E}_k, \tag{7}$$

$$D_i = e_{ikl}\varepsilon_{kl} + \varepsilon^s_{ik}\mathbf{E}_k. \tag{8}$$

In the above equations, $C^{\mathbf{E}}_{ijkl}$ demands for elastic material constants and e_{kij} is the piezoelectric stress constants.

The boundary conditions for fluid-solid interaction consist of a no slip condition and interface continuity in traction replaced by a continuity of stresses:0

$$\boldsymbol{\sigma}^s_{ij} n^s_j + \boldsymbol{\sigma}^F_{ij} n^s_j = 0, \tag{9}$$

where n is the outward unit vector, and s and F represent solid and fluid properties, respectively.

3. Multi-field analysis

A schematic of the micropump components is shown in Figure 1. In this study, commercial software packages, Ansys and Ansys-CFX, were adopted for the simulation of the fluid flow and the structural part, respectively. The generated grid for the fluid domain consists of tetrahedral elements and it is smoothly adapted for high velocity gradient regions. The simulation includes almost all the physical aspects of the working mechanism, such as the piezoelectric effect and two way fluid-solid interactions. In other words, there are two different levels of multiphysics behavior containing electrical-structural coupling and structural-fluidic coupling effects considered in this paper. A node-to-face mapping is used to interpolate loads between dissimilar meshes on either side of the coupling interface. Each field solver advances through a sequence of multifield time steps and stagger (coupling) iterations within each time step. During every stagger iteration, each field solver collects the loads that it requires from the other field solvers and then solves its physics fields.

In the proposed micropump, the PZT is 5 mm in diameter and 200 μm in thickness. The vibrating diaphragm is 6 mm in diameter and 300 μm in thickess. The depth of the planar micropump is 120 μm. The peak to peak driving voltage is the same for all cases and is equal to 80 V. The main dimensional parameters for the nozzle valves are shown in Figure 2, which are chosen for an optimized condition based on Olsson's experiments [3]. Material properties used in the analysis of the micropump are shown in Table 1. The pressures at the inlet and outlet of the micropump are atmospheric pressure. The time step was chosen as 1/25 of the period time and was checked to be independent from the final solution.

4. Results and discussion

The solution is converged after 3 or 4 periods in most cases. The pump flow is calculated at the outlet valve. The maximum membrane displacement and net flow rate versus time are reported in Figures 3 to 6 for different wave shapes and a frequency of 100 Hz. The net flow rate is avraged over a period. For simplicity and better comparison, we assume that when the chamber is upward and the displacement is positive, the flow direction has also a positive sign, which causes the flow to stream into the chamber. Because the driving frequency is low enough, the membrane displacement follows the same manner as the input voltage, except

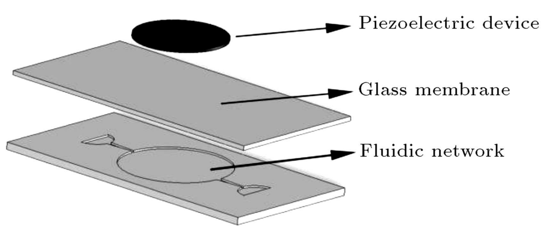

Figure 1. A schematic of the micropump.

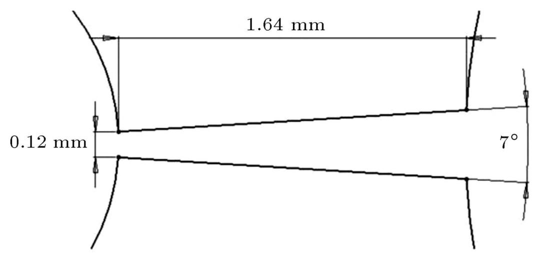

Figure 2. The dimensional parameters for nozzle valve.

Table 1. Materials and fluid properties.

Material	Property	Value
PZT4	Piezoelectric stress tensor e (C/m^2)	$\begin{bmatrix} 0 & 0 & -4.1 \\ 0 & 0 & -4.1 \\ 0 & 0 & 14.1 \\ 0 & 10.5 & 0 \\ 10.5 & 0 & 0 \\ 0 & 0 & 0 \end{bmatrix}$
	Realative permittivity (F/m)	$\begin{bmatrix} 804.6 & 0 & 0 \\ 0 & 804.6 & 0 \\ 0 & 0 & 659.7 \end{bmatrix} \times 10^{-11}$
	Elastic matrix C^E (N/m^2)	$\begin{bmatrix} 13.2 & 7.3 & 7.1 & 0 & 0 & 0 \\ 7.3 & 13.2 & 0 & 0 & 0 & 0 \\ 7.1 & 7.1 & 11.5 & 0 & 0 & 0 \\ 0 & 0 & 0 & 26 & 0 & 0 \\ 0 & 0 & 0 & 0 & 26 & 0 \\ 0 & 0 & 0 & 0 & 0 & 3 \end{bmatrix} \times 10^{10}$
Glass	Density ρ (kg/m^3)	2600
	Young's modulus (GPa)	6.27E10
	Poisson ratio	0.2
Water	Density (kg/m^3)	997
	Viscosity (Ns/m^2)	8.9E-4

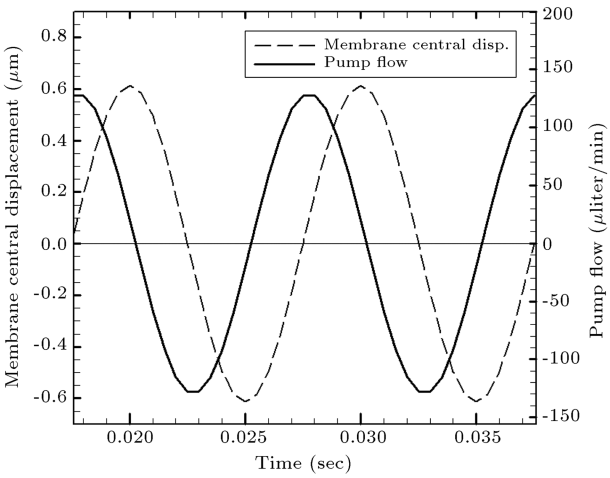

Figure 3. Pump flow and membrane displacement versus time for sinusoidal excitation.

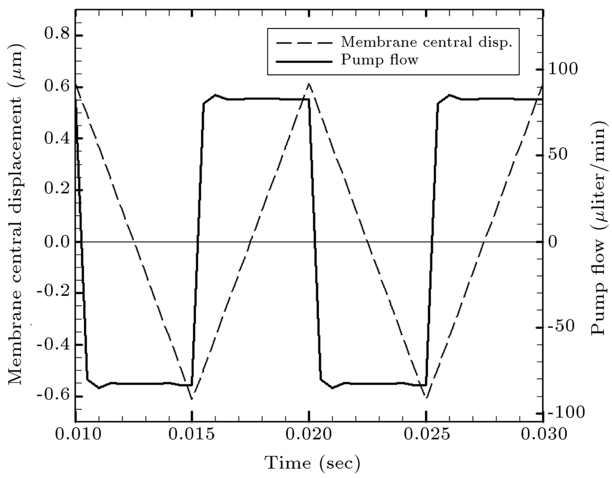

Figure 4. Pump flow and membrane displacement versus time for triangle excitation.

for small deviations after sudden jumps in square and sawtooth excitations, as shown in Figures 5 and 6. For this reason, the voltage distribution is not included in the diagrams.

Figures 3 and 4 show that there is a phase difference between displacement and flow rate for sinusoidal and triangle excitations. In other words, the phase of pump flow lags behind the displacement phase by about a quarter of a period. This can be easily explained if one considers the derivative of the displacement diagram. Indeed, pump flow follows the same manner as membrane velocity. Even for sawtooth and square waves, the flow behavior is rather similar to the derivative of the displacement.

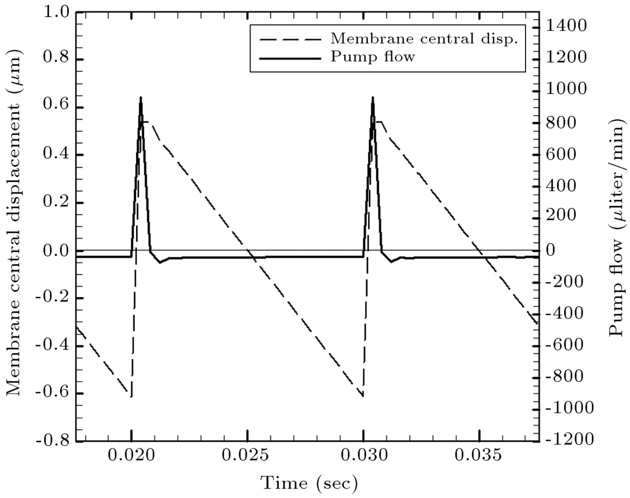

Figure 5. Pump flow and membrane displacement versus time for sawtooth excitation.

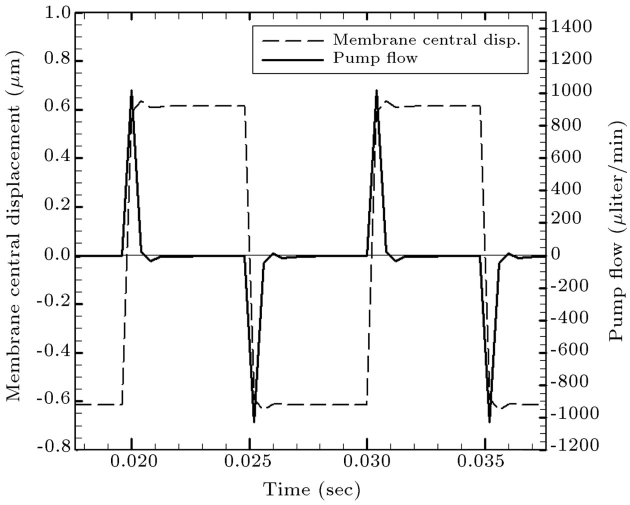

Figure 6. Pump flow and membrane displacement versus time for square excitation.

From Figure 6, it is also evident that there is a sudden change in flow rate at half the period time, while very low pump flow is attained along the cycle. For better understanding of this behavior, let us consider the flow inside the pump for a square wave and one period of time. Velocity vectors in the micropump centerplane at different times of one period is depicted in Figure 7. At $t = 0.030$ sec, there is a sudden upward movement for the membrane. It causes the flow to stream from both inlet and outlet into the chamber with maximum velocity. Therefore, flow velocity is high at the throat and entrance of the nozzles (that is, in regions A and C (Figure 7)). From velocity vectors, distribution at the middle part of the half cycle, e.g. $t = 0.033$ sec in Figure 7, it can be easily seen that high velocity is more prominent in region C just after the jet enters the chamber. While the membrane position is nearly constant during the

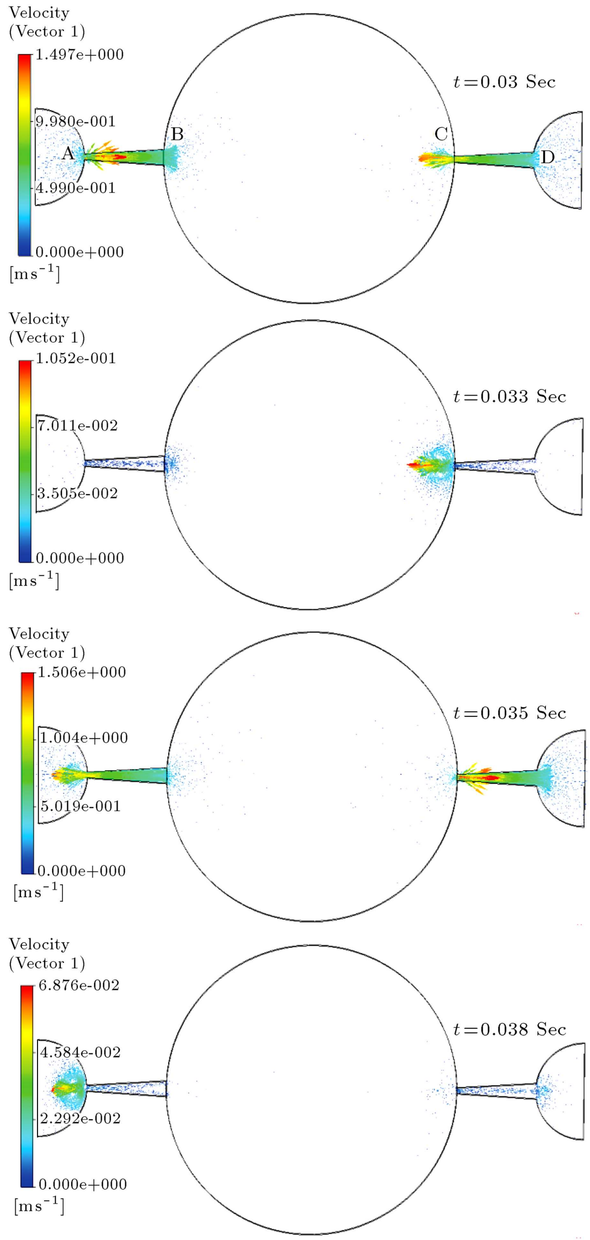

Figure 7. Top view of the proposed micropump and velocity vectors distribution at the centerplane for different times during a period.

half cycle between $t = 0.030$ and $t = 0.035$ sec, the vortices grow instantly in region C after the sharp rise in membrane displacement. The summit starts to move towards the center of the chamber with time increment. As a result, strong vortices block the jet flow, and backward streams start to produce. This is why the pump flow reaches a plateau with very low flow rate between $t = 0.030$ and $t = 0.035$ sec in Figure 4. For the next half cycle, the chamber behaves like a source and pushes the flow out of the pump. At this time, the flow velocity is high, mostly in region A.

In contrast to the sinusoidal waveform, whose membrane position changes dynamically with the time,

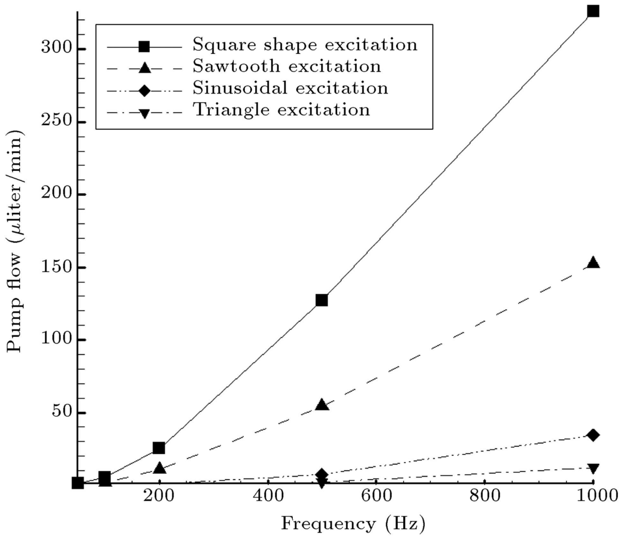

Figure 8. Pump flow versus driving frequency for different waveforms.

in square wave one, the flow has enough time to form the vortices at high velocity gradient regions because of consistency in membrane position. Consequently, strong vortices obstruct the flow in the region and backward streams grow rapidly. Considering the whole phenomena for a full cycle, one can conclude that the more sharp jump in wave form, the more pump flow can be attained at the outlet. In other words, sharp waveform excitation assists inlet and outlet valves in diodicity property. In the first half cycle, large vortices are generated in region C, which result in a lower flow rate in comparison with the next half cycle in which the flow is in an opposite and favorite direction. The same scenario is repeated for region A during a cycle.

The mean pump flow versus working frequency is depicted in Figure 8 for different waveforms. This analysis is justified, implementing a wide range of driving frequency from 50 to 1000 Hz. It is seen that the upward trend of flow rate for square excitation is hastened at high frequencies and there is a large difference in flow rate compared to sinusoidal and triangular ones.

The above mentioned phenomenon of vorticity generation can be used to explain what lies behind the maximum flow rate gained for square excitation. The sawtooth waveform also produces large amount of flow rate compared to the sinusoidal and triangle ones. Similarly, sharp edges with a steep slope cause the same phenomenon explained for the square wave.

Figure 9 shows streamline patterns at different times for frequencies of 100 Hz and 1000 Hz. In this figure the sinusoidal signal is used for driving voltage, and the flow patterns were ploted for four major membrane positions during one period. As mentioned before, for square wave excitation, backward streams magnify the pump ability to push more flow out of the chamber. As seen in Figure 9, there are no major vorticies in the fluid region for sinusoidal excitation and a frequency of 100 Hz. Meanwhile, the streamlines show that backward flow is more notable when the driving frequecy is 1000 Hz. Here, the flow behavior is the same as that explained for square excitation at 100 Hz. Therefore, considering the generated vortices in the flow will help to explain the increment of pump flow with frequency rising for sinusoidal excitation. Nevertheless, in this case, the vortex generation itself is due to larger membrane displacement at higher frequencies.

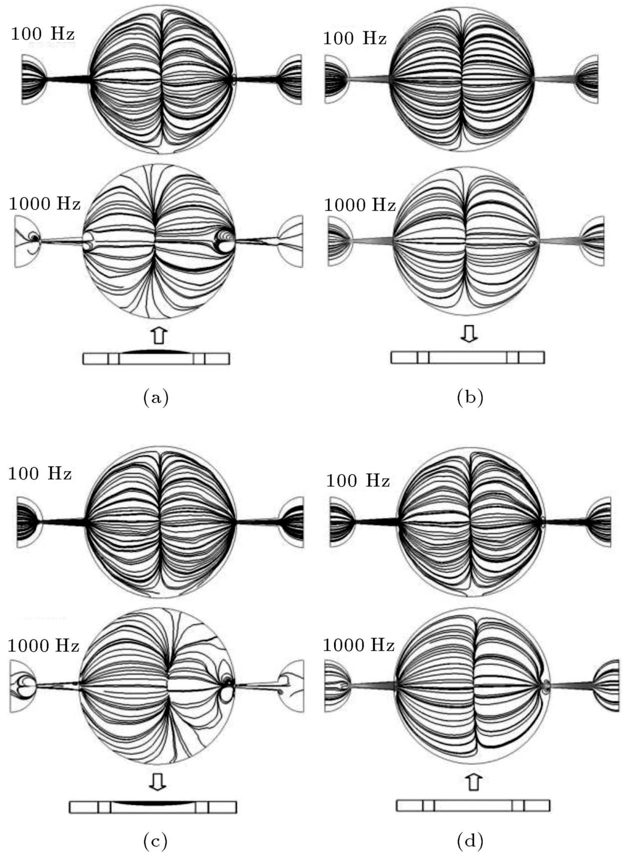

Figure 9. Streamline patterns for two different frequencies of sinusoidal excitation at several times: a) Membrane in crest position; b) membrane in medial position moving down; c) membrane in trough position; and d) membrane in medial position moving up.

A micropump with a cylindrical chamber, like that reported by Izzo et al. [13], in 2007, was used to validate the accuracy of the developed model in simulation of micropump behavior. In Figure 10, the maximum flow rate versus driving frequency is depicted. It shows good agreement between experimental data and simulation results. It is also evident that numerical findings have given a correct intuitive peak frequency value. Therefore, the coupled finite element-finite volume method can be used for further investigations in the future.

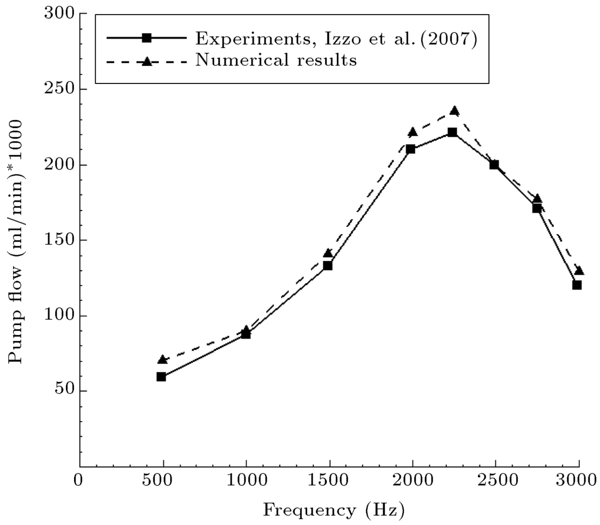

Figure 10. Pump flow versus driving frequency at zero pressure.

5. Conclusions

In this study, a three-dimensional model of a piezoelectric micropump with nozzle-diffuser valves was modeled numerically. A transient analysis was carried out considering tri electro-mechanical-fluidic coupling effects. However, the main concern is regarding waveform influence on the performance of the pump in a wide range of driving frequencies. The results are summarized as follows:

1. Square wave excitation causes the most remarkable amount of flow rate among all investigated cases for the entire range of frequencies studied. The story behind this behavior can be explained by the vortices generated in the flow.
2. Among studied waveforms, sinusoidal excitation seems to have a notable phase difference between flow and membrane displacement at the working frequency.
3. At low working frequency, the membrane displacement mostly follows the same manner as excitation voltage. For higher frequency, the membrane may behave quite differently.
4. Because a sawtooth wave also can pump a large amount of flow during a period, one can conclude that the deeper the sharp exists in the waveform, the more pump flow can be obtained.
5. As the working frequency increases, larger membrane displacement is gained. Consequently, it causes a steady rise in net pump flow rate. The upward trend in flow rate for square excitation is hastened at high frequencies and there is a large difference in the flow rate compared to sinusoidal and triangle ones.
6. At higher frequencies, vortices grows in fluid flow and magnify the ability of the pump to push more flow out of the chamber.
7. The validation process shows that the present model can predict the resonance behavior of micropumps with good accuracy.

Abbreviations

MEMS	Micro-Electro-Mechanical Systems
NVP	No-Moving-Part
PZT	Lead Zirconate Titanate

References

1. Stemme, E. and Stemme, G. "A valveless diffuser/nozzle-based fluid pump", *Sensors and Actuators A*, **39**, pp. 159-167 (1993).
2. Forster, F.K., Bardell, R.L., Afromowitz, M.A., Sharma, N.R. and Blanchard, A. "Design, fabrication and testing of fixed-valve micro-pumps", *Proc. ASME Fluids Eng. Div. ASME*, **234**, San Francisco, pp. 39-44 (1995).
3. Olsson, A., Larsson, O., Holm, J., Lundbladh, L., Ohman, O. and Stemme, G. "Valve-less diffuser micropumps fabricated using thermoplastic replication", *Sensors and Actuators A*, **64**, pp. 63-68 (1998).
4. Olsson, A., Stemme, G. and Stemme, E. "Numerical and experimental studies of flat-walled diffuser elements for valve-less micropumps", *Sensors and Actuators A*, **84**, pp. 165-175 (2000).
5. Ullmann, A., Fono, I. and Taitel, Y. "A piezoelectric valve-less pump-dynamic model", *Journal of Fluids Engineering*, **123**, pp. 92-98 (2001).
6. Ahmadian, M.T. and Mehrabian, A. "Design optimization by numerical characterization of fluid flow through the valveless diffuser micropumps", *Journal of Physics: Conference Series*, **34**, pp. 379-384 (2006).
7. Li, S. and Chen, S. "Analytical analysis of a circular PZT actuator for valveless micropumps", *Sensors and Actuators A*, **104**, pp. 151-161 (2003).
8. Ahmadian, M.T., Saidi, M.H., Mehrabian, A., Bazargan, M. and Kenarsari, S.D. "Performance of valveless diffuser micropumps under harmonic piezoelectric actuation", *8th Biennial ASME Conference on Engineering Systems Design and Analysis*, Torino, Italy, pp. 693-699 (2006).
9. Yang, K.S., Chen, I.Y., Chien, K.H. and Wang, C.C. "A numerical study of the nozzle/diffuser micropump", *J. Mechanical Engineering Science*, **222**, pp. 525-533 (2008).
10. Hou, W., Das, B., Jiang, Y., Qian, S., Zheng, X., Pi, X., Yang, J., Liu, H., Zheng, J. and Zheng, Z. "Simulation of the diaphragm properties of a PZT-based valveless micropump", *Proceedings of the 3rd IEEE Int. Conf. on Nano/Micro Engineered and Molecular Systems*, Sanya, China, pp. 449-452 (2008).

11. Cui, Q., Liu, C. and Zha, X. "Simulation and optimization of a piezoelectric micropump for medical applications", *Int. J. Adv. Manuf. Technol.*, **36**, pp. 516-524 (2008).

12. Yanfang, G., Guoxian, Z., Jicun, R. and Zhihua, G. "Fabrication and experiment studies of the piezoelectric micropump with saw-tooth microchannel", *CORD Conference Proceedings*, **2**, Shanghai, China, pp. 733-737 (2009).

13. Izzo, I., Accoto, D., Menciassi, A., Lother, S. and Paolo, D. "Modeling and experimental validation of a piezoelectric micropump with novel no-moving-part valves", *Sensors and Actuators A*, **133**, pp. 128-140 (2007).

Biographies

Ebrahim Kolahdouz obtained his MS degree in Mechanical Engineering from Isfahan University of Technology, Iran. His thesis was on the numerical simulation and experimental validation of a piezoelectric micropump with modified Tesla valves. He is currently completing his PhD degree studies on Modelling the Electro-hydrodynamics of Lipid Vesicles, at SUNY, Buffalo, USA.

Kazem Mohammadzadeh was born in 1988, in Iran. He received his BS degree in Fluid Mechanics from the University of Birjand, in Iran, and his MS degree in Thermo Fluids from Isfahan University of Technology, Iran. He is currently instructor at Foolad Institute of Technology, Iran, and a PhD degree student of Mechanical Engineering at Tarbiat Modares University, Tehran, Iran. His research interests include microfluidics, heat transfer, micropumps, and PEM fuel cells.

Ebrahim Shirani obtained his PhD degree in Mechanical Engineering from Stanford University, USA, in 1981. He is currently faculty member at Foolad Institute of Technology, Iran, and Professor Emeritus in the Mechanical Engineering Department at Isfahan University of Technology, Iran. His research interests include CFD, micro-nano fluid flows, turbulence, turbomachinery and biofluid mechanics.

Saeed Ziaei-Rad obtained his PhD degree in Mechanical Engineering from Imperial College, London, UK, in 1997, and is currently Professor in the Mechanical Engineering Department at Isfahan University of Technology, Iran. His research interests include vibration of smart structures and rotating machinery, experimental and analytical modal analysis, computational micro and nano-mechanics, advanced composite materials.